Available online at www.sciencedirect.com
SCIENCE DIRECT®
Physics and Chemistry of the Earth 31 (2006) 154–163
PHYSICS and CHEMISTRY of the EARTH
www.elsevier.com/locate/pce

Satellite thermal IR phenomena associated with some of the major earthquakes in 1999–2003

Dimitar Ouzounov [a,*], Nevin Bryant [b], Thomas Logan [b], Sergey Pulinets [c], Patrick Taylor [d]

[a] NASA GSFC/SSAI, MS 698, Greenbelt, MD 20771, USA
[b] NASA JPL/ Caltech, Pasadena, CA 91109, USA
[c] Institute of Geophysics, UNAM, Mexico
[d] NASA GSFC, MS 698, Greenbelt, MD 20771, USA

Accepted 6 February 2006

Abstract

Satellite thermal infrared (TIR) imaging data have recorded short-lived anomalies prior to major earthquakes and associations with fault systems. Others have proposed that these signals originate from electromagnetic phenomena associated with pre-seismic processes, causing enhanced IR emissions, that we are calling TIR anomalies. The purpose of this exploratory study is to verify if TIR anomalies can be found in association with known earthquakes by systematically applying satellite data analysis techniques to imagery recorded prior-to and immediately after large earthquakes. Our approach utilizes both a mapping of surface TIR transient fields from polar orbiting satellites and co-registering geosynchronous weather satellites images. The significance of these observations was explored using data sets of recent worldwide strong earthquakes (1999–2003) and the techniques used to capture the trace of TIR anomalies.

Keywords: Remote sensing and electromagnetic phenomena; Satellite thermal image; Earthquake dynamics and mechanism; Creep and deformation

1. Introduction

Satellite thermal imaging data have not only revealed stationary (long-lived) thermal anomalies associated with large linear structures and fault systems in the Earth's crust (Carreno et al., 2001; Fizzola et al., 2004) but also transient (short-lived) features prior to major earthquakes (Tronin et al., 2004a,b; Tramutoli et al., 2005). These short-lived anomalies: (1) typically appear 4–14 days before an earthquake; (2) affect regions of several to tens of thousand square km; (3) display a positive deviation of 2–4 °C or more; and (4) die out a few days after the event. The rapidity with which these temperature excursions occur suggests that they cannot be due to thermal variations caused by a heat pulse rising from within the Earth. Their spatial extent and temporal evolution may be dependent on meteorological conditions (Tramutoli et al., 2005), local geology and seismo-tectonics conditions.

In the past, several processes have been considered as possible contributors to the transient short-lived "thermal anomalies": (a) rising fluids that would lead to the emanation of warm gases (Salman et al., 1992; Gorny et al., 1988); (b) rising well water levels and CO_2 spreading laterally and causing a "local greenhouse" effect (Qiang et al., 1991; Tronin et al., 2002; Tramutoli et al., 2005); (c) activating positive-hole pairs during rock deformation (Freund, 2002); (d) radon ionization of the near surface air and latent heat exchange due to variations of humidity (Pulinets et al., 2006a).

Two other methods for TIR analysis related to large earthquakes have been recently developed. The single image approach, comparing pre (vs post) earthquake satellite TIR imagery (Gorny et al., 1988; Singh et al., 2002;

* Corresponding author. Tel.: +1 301 614 6498; fax: +1 301 614 6522.
E-mail address: ouzounov@core2.gsfc.nasa.gov (D. Ouzounov).

1474-7065/$ - see front matter © 2006 Elsevier Ltd. All rights reserved.
doi:10.1016/j.pce.2006.02.036

Tronin et al., 2002, 2004a). The robust TIR technique – pixel temperature variance from long-term scene threshold temperatures used to identify "hot" (Tramutoli et al., 2001, 2005) areas.

Of late two different techniques for detecting TIR anomalies related to major earthquake were proposed using sub pixel level of co-registration and geo-referenced all imagery data from GOES, Meteosat, AVHRR and Landsat (Bryant et al., 2003; Di Bello et al., 2004) and multi-spectral IR component analysis of polar orbit satellite Terra/MODIS and Aqua/MODIS by using split window LST for 11 μ (Ouzounov and Freund, 2004). A similarity of both techniques is that "anomalous" effect was defined as a deviation from a pre-existing reference field (usually a multi-year mean value). Others have also observed at distances of 200–1000 km from the epicenters, from two weeks to a few hours before the event (China, Japan, Russia, Turkey, Mexico and Greece; Liu et al., 2000; Tramutoli et al., 2001; Tronin et al., 2002).

Despite the multitude of previous models, no comprehensive explanation acceptable to the science community has been proposed. In this paper we review the results of recent investigations and analyze a large number of satellite acquisitions acquired over a short period of time (weeks) in the regions of recent earthquakes and discuss the evidence of transitory thermal anomalies.

2. Data and methodlogy description

2.1. Data

Shortly before the Hector Mine, California earthquake (Magnitude 7.1 at 09:47 UTC, 02:47 local time, on 16 October 1999), Landsat-7 (Scene ID: L71040036_03619991015) passed over the epicenter 15 h prior to the earthquake (Bryant et al., 2003). Moreover, Robert Crippen of JPL observed that the Landsat-7 thermal infrared band recorded the highest radiance values in the 185×185km scene near the fault epicenter (see Fig. 1). Subsequent analysis of polar orbiting (NOAA/AVHRR) and geosynchronous (GOES-10) weather satellite imagery (October 15 and 15, 1999) showed this area to have a significantly elevated apparent ground surface temperature when compared to the same time frame in the following year (Fig. 1). A review of the weather records showed that the prevailing air temperature had been declining from the 15th to 16th

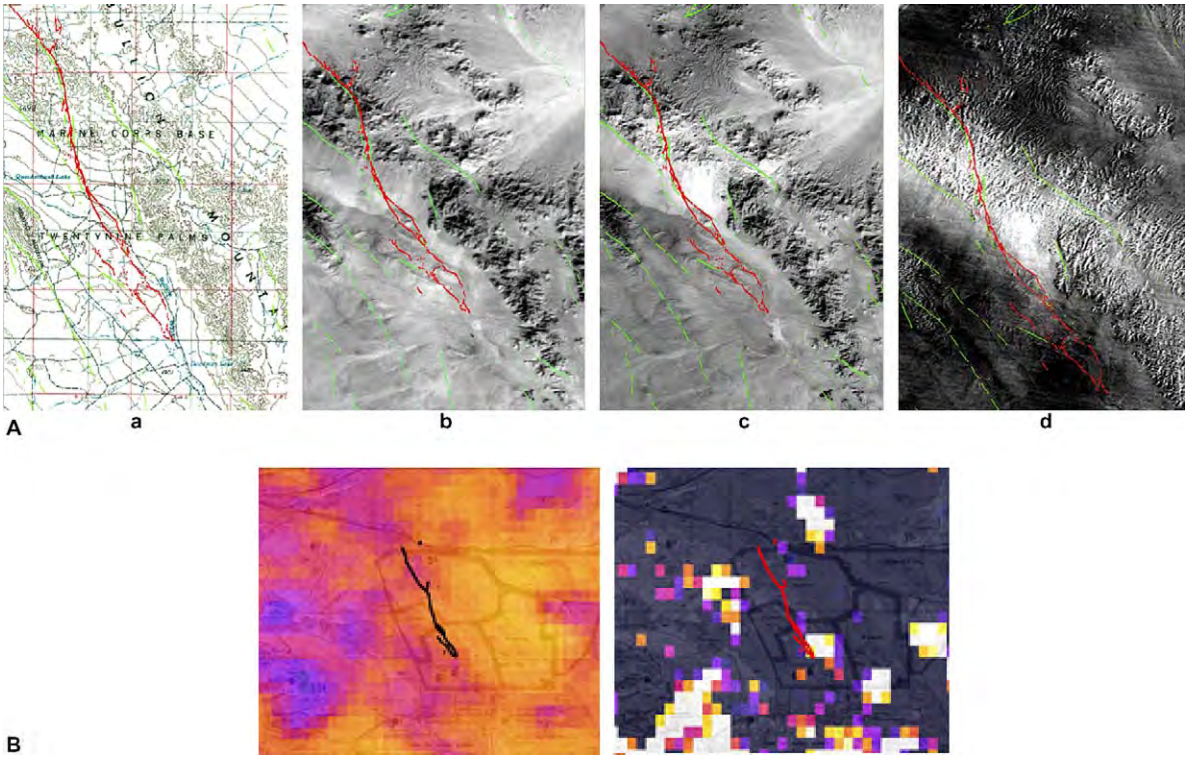

Fig. 1. (A) Thermal anomaly observed on 15 October 1999, 15 h prior to the Hector Mine, CA Earthquake (Note: Landsat thermal band is not directly calibrated with temperature, images are relative temperatures). (a) Location Map provides orientation with an overlay graphic (in red) of the surface trace of the fault. (b) 20 October 1998, landsat image (one year prior to the earthquake). (c) 15 October 1999, landsat image acquired 15 h prior to earthquake. Bright pixels relatively hotter. (d) Difference image of Landsat images taken one year apart. Brighter areas are warmer in 1999. (B) Temperature and regression slope maps of Hector Mine event derived from GOES imagery. The temperature map (left) depicts the ground surface temperature average for the three hours following the Hector Mine earthquake, and range from cooler blue/purple (272 K) through hotter red/yellow (297 K). Temperature averages are made over six half-hour time periods: 3:00–6:30 am local time for Hector Mine, CA; The regression slope maps (right) range from negative (i.e. decreasing temperatures over the three hour time period) as dark gray, to ranges of temperature increases where purple = low (1–2 °C) and white = high (3–5 °C). The location of the faults are noted as black and red graphic overlays.

of October and the California desert region was cloud-free for an extended period of time. The apparent measurable ground temperature increases were observed to be of limited area extent near the fault only hours prior to the earthquake and then observed over a much broader area for a short duration afterwards. The rare event of a Landsat overpass just 15 h prior to an earthquake has not been repeated. The Hector Mine study demonstrated the need for regional level, time series of satellite imagery over an extended period. Therefore we have analyzed NOAA geosynchronous and polar orbiting weather satellites and the NASA daily revisit satellites Aqua and Terra. We systematically co-registered weather satellite images at the sub-pixel level or computed multi year residual of transient surface temperature by polar orbiting satellite data and then determining if statistically significant responses had occurred prior to an event. These techniques apply best to the use of the geosynchronous weather satellites (GOES, Meteosat, and GMS), where images are taken every thirty minutes from polar orbits (Terra/Aqua MODIS, NOAA/AVHRR). Use of the geosynchronous satellites also reduces the potential for miscalculating trends due to weather front movement or local cloud/fog formation. The polar orbiting satellites have better resolution (1 km vs 5 km) and better signal-to-noise ratios, but only acquire images twice during an evening, thereby making trend analysis more difficult.

The Earth's surface receives energy from the Sun as solar radiation in the visible range (380–625 nm) and emitted back (thermal emission) in the IR range. The atmosphere is mostly transparent in 8–14 μm band and the two different satellites were used for analysing the thermal non-stationary anomalies: Terra and Aqua – polar orbit (Sun Synchronized) and GOES/Meteosat – Geostationary (Geo synchronized) orbit satellites have received data in this window. The Moderate Resolution Imaging Spectroradiometer (MODIS), a major NASA EOS instrument, was launched aboard the Terra satellite on December 18, 1999 for global monitoring of the atmosphere, terrestrial ecosystems, and oceans. On May 4, 2002, a similar instrument was launched on the EOS-Aqua satellite. MODIS, flying on these two satellites, complement each other by providing observations at different local times. With its 2330 km viewing swath width, MODIS on Terra and Aqua provides almost complete dual global daily coverage in 36 spectral bands between 0.415 and 14.235 μm with spatial resolutions of 250 m (two bands), 500 m (five bands), and 1000 m (29 bands). The MODIS radiance data provide improved information about the physical structure of the Earth's atmosphere and surface (http://www.modis.gsfc.nasa.gov). The geostationary and polar-orbiting weather satellites GOES or Meteosat provide continuous monitoring that is necessary for intensive data analysis. The geosynchronous orbital plane is at about 35,800 km, high enough to allow the satellites a full-disc view of the Earth. For the all five channels (VIS to 0.71 μm; 3.73–4.07 μm; 5.8–7.3 μm; 10.2–11.2 μm and 13.0–13.7 μm) images with pixel sizes of 1 km, 4 km or 8 km can be obtained. By staying above a fixed spot on the surface, the GOES satellites are designed to provide a constant vigil for atmospheric "triggers" of severe natural hazard events and violent weather (http://www.oso.noaa.gov/goes/index.htm).

2.2. Applied techniques for TIR anomaly analysis

This work is concentrated on four TIR anomaly studies (see Table 1) using the two combined techniques and their analysis. We do not intend to perform a complete review of the latest techniques for TIR analysis or to address a theory for the generation of TIR phenomenon.

Two techniques were selected to perform the TIR analysis: (A) co-registration and geo-referenced on sub pixels to provide radiation data closest to the fault lines at sub pixel level; and (B) using the split windows LST and SST estimate in the near epicentral area (100×100 km) to obtain spatial information (with 1 km pixel resolution) about any surface temperature change prior to the earthquake.

(A) For co-registering geosynchronous weather satellite observations a new set of automatic procedures were developed at JPL. These accommodate all properties particular to nighttime weather satellite observations. Corrections for spacecraft and sensor ephemeris and the horizontal displacement due to elevation were all accounted for. Final adjustments for minor satellite deviations (related to roll, pitch, and yaw) were made by using image-to-image tie point correlations. Reliance upon visual clues in an image (frequently the subject of debate in the past) is not required.

Co-registered geosynchronous weather satellite observations were used to identify apparent ground surface tem-

Table 1
List of the earthquakes presented into this analysis

Name	Date (mm/dd/yyyy)	Geographic Lat/Lon	Time (UTC)	Mw	H (km)	Satellite	Focal mechanism
Izmit, Turkey	08/17/1999	40.75N/29.86E	00:01:39	7.8	17.0	Meteosat	Strike-slip fault, foreshocks
Hector Mine, CA, USA	10/16/1999	34.59N/116.27W	09:46:00	7.1	5.0	LANDSAT, NOAA/AVHRR GEOS	Strike-slip fault, foreshocks
Bhuj, Gujarat, India	01/26/2001	23.40N/70.32E	03:16:41	7.9	23.6	Meteosat, MODIS	Thrust Fault, no foreshocks
Kunlun, Tibet, China	11/14/2001	36.014N/90.504E	09:26:10.20	7.7	5.0	Meteosat	Strike-slip
Colima, Mexico	01/21/2003	18.81N/103.89W	2:06:35	7.8	24.0	MODIS	Strike-slip
Boumerdes, North Algeria	05/21/2003	36.90N/3.71E	18:44:19	6.8	10.0	Meteosat, MODIS	Thrust Fault and Strike-slip, no foreshocks

perature trends for each individual time series pixel-set in the composite of half-hour intervals for each image acquired over the course of a night. Night observations were selected so as to avoid concerns with solar thermal effects. This technique relies on the cooling of the ground after sunset. The repeated measurements from the geosynchronous weather satellite (every 30 min) allows us to monitor apparent ground surface temperature trends over various time segments of the night through the application of slope regression analysis to co-registered pixel sets of 10–20 half-hourly scenes (see Fig. 2). The use of regression slope values and graphed plots of selected nighttime sequences revealed apparent ground surface temperature increases/decreases that were in contrast to the expected natural diurnal nighttime temperature trends, thus indicating the location of a "thermal anomaly". The regression slope values were prepared for the satellite measurements made after the rapid cooling at sunset (usually ~8 pm local time) until sunrise (usually ~6 am local time).

(B) Surface Temperature anomalies retrieved form polar orbiting satellites. Using nighttime emissions from the Earth's surface, we analysed the MODIS Land Surface Temperature and Emissivity (LST/E) data (MOD11A1) over 90 days by means of the 11–12 μm emissivity ratio (mid IR channels 31/32) covering areas of 100×100 km and we looked for correlations between the atmospheric dynamics and any variations of the Earth's surface prior to the major events.

MODIS LST products provide per-pixel temperature and emissivity values (only over the land, sea is masked). Temperatures are extracted in degrees Kelvin with a view-angle dependent algorithm applied to direct observations. This method yields 1 K accuracy for materials with known emissivities (Justice et al., 1998). The algorithm most suitable for land-cover types that have stable emissivities known to within 0.01 (Wan and Li, 1997) was used in this work for processing MODIS data in bands 31 and 32 in the split-window at 11 and 12 μm, respectively.

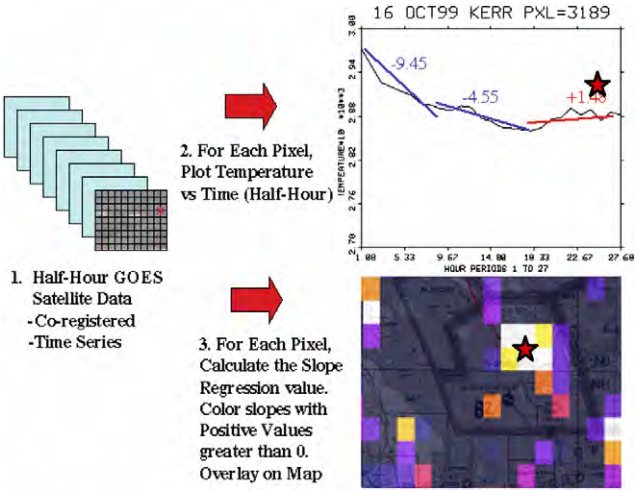

Fig. 2. Methodology used for: (1) preparing time-series plots; (2) calculating regression slope values for a set of observations taken at 30 min intervals; and (3) producing a regression slope map for an area of interest.

We define an LST anomaly as a difference between spatial daily root mean square (RMS) values and mean value in an area of $M \times N$ km^2 centred at the epicenter and located on the stress-released fault.

$$\Delta \mathrm{LST}^i = \mathrm{LST}^i_{\mathrm{RMS}} - \overline{\mathrm{LST}}_{\mathrm{RMS}} \quad (1)$$

Here $\mathrm{LST}^i_{\mathrm{RMS}}$ – daily area variation of LST, $\mathrm{LST}_{\mathrm{RMS}} = \sqrt{\frac{\sum_{x=1,y=1}^{M,N} \mathrm{LST}^2_{xy}}{MN}}$, M and N – size of the analyzing area (usually is 100×100 km) and $\overline{\mathrm{LST}}_{\mathrm{RMS}}$ mean value for the entire time interval of analysis $i = 1, D$ (D – number of days, usually 60, or 90) days.

The split-window algorithm yearly ΔLST anomaly, for nighttime within $M \times N$ area around the epicenter was defined as residuals of the two-year (or multiple years) data analysis for the pre defined time interval of D days.

$$\Delta \mathrm{LST}^i_A = \Delta \mathrm{LST}^{xxxx}_i - \Delta \mathrm{LST}^{yyyy}_i \quad (2)$$

where $i = 1, D$ days, $\Delta \mathrm{LST}^{xxxx}_i$ and $\Delta \mathrm{LST}^{yyyy}_i$ are the yearly estimate according (1).

We are exploring the idea also that several physical parameters of the ocean surface such as the sea surface temperature (SST) or anomalous chlorophyll and salinity values that can be derived from IR satellite observations may also correlate with the location of marine earthquakes. Large-scale (~100 km) SST anomalies with negative temperature excursions (up to −5 °C compared to background) were detected for the first time over the epicentral regions of strong underwater earthquakes during an analysis of SST maps and comparison with the near-real time earthquake catalogue (Nosov, 1998). The newest data from Terra and Aqua /MODIS make it possible to reveal repeatable pattern of SST (temperature is defined only over the sea, land is masked) anomalies in the same area with 1 K resolution connected with main earthquake activity ($M > 5$). In addition 2-D method of median polish (MP) (Cressie, 1993) for spatial analysis has been introduced to the MODIS SST grid. To validate the relevance of SST decrease exploratory data analysis based on MP has been applied to the 4.5 km nighttime griddled SST data in order to decompose into large-scale and small-scale variations (see Section 3.2 and Fig. 7).

3. Results

The Meteosat geosynchronous weather satellites used to observe these earthquakes have only one thermal band (10.5–12.5 μ). This restricted our efforts to utilize these data taken at half-hour intervals as a time series, and not as an absolute temperature threshold event. A review of meteorological data showed that weather effects (clouds or haze and air temperature) were stable over the areas of interest, and did not adversely affect the Meteosat observations. The result of the new analytic procedures has been the

observance of apparent heating trends close to epicenters in satellite data acquisitions a few days to a few hours prior to an earthquake. A heating trend in this context implies that observations along known fault-lines show a much-reduced 'temperature' decline through the evening after sunset, or in some cases an actual 'temperature' increase during the course of the night prior to an earthquake occurrence.

In case of polar orbit satellite data an area (100 × 100 km) around the epicenter was established to study the deviation of surface temperature during the nighttime periods. Cloudy pixels were excluded and anomalous values of temperature and spatial deviation were defined in comparison with baseline values build for the same time interval through multiple years.

3.1. Bhuj (Gujarat), India, January 26, 2001, M7.7

The Bhuj, India, earthquake was chosen because it occurred during a period of clear weather. Observations with the Meteosat thermal infrared band showed a thermal anomaly prior to the earthquake (at 08:46 am local time, January 26, 2001) along the western portion of the fault lineament determined by (Yagi, 2001) (there were no surface ruptures). Fig. 3 shows that the average apparent ground surface temperature over the ten-hour period of the night of January 25th became more elevated when compared with January 24th. The ground surface temperature record on the night following the earthquake, January 26th, appears to have remained as high as the previous night. This may be associated with the broad area of liquefaction experienced. Maps of the pixel regression slopes show that the build-up in apparent ground surface temperature was widespread after the initial cooling at sunset on the night of January 25th (Fig. 3 and Table 2). On the basis of polar orbit data on 20 January (Terra/MODIS crossing Gujarat at ~6AM, 6PM UTC), as shown in Fig. 1, a pronounced LST increase is observed for the area close to the epicenter of the 26 January magnitude 7.7 event. We see a LST anomaly pattern, which appears to have statistical significance, i.e. a positive temperature excursion with a maximum of +4 °C compared to the background (Ouzounov and Freund, 2004). The LST anomaly (Fig. 4) began on 20/21 January 2001, 5–6 days before the event, close to the main tectonic fault but it did not spread beyond 200 km from the epicenter location. In Fig. 4 is shown the major seismo-tectonic fault system related to the quake. Main stress was released along the Katrol Hill and Mainland faults (Singh and Ouzounov, 2003). In Fig. 4 are shown the nighttime LST Terra/MODIS images over the epicentral area on January 18, 20, 21 and 22, 2001. Contours of those lineaments were separated with anomalous

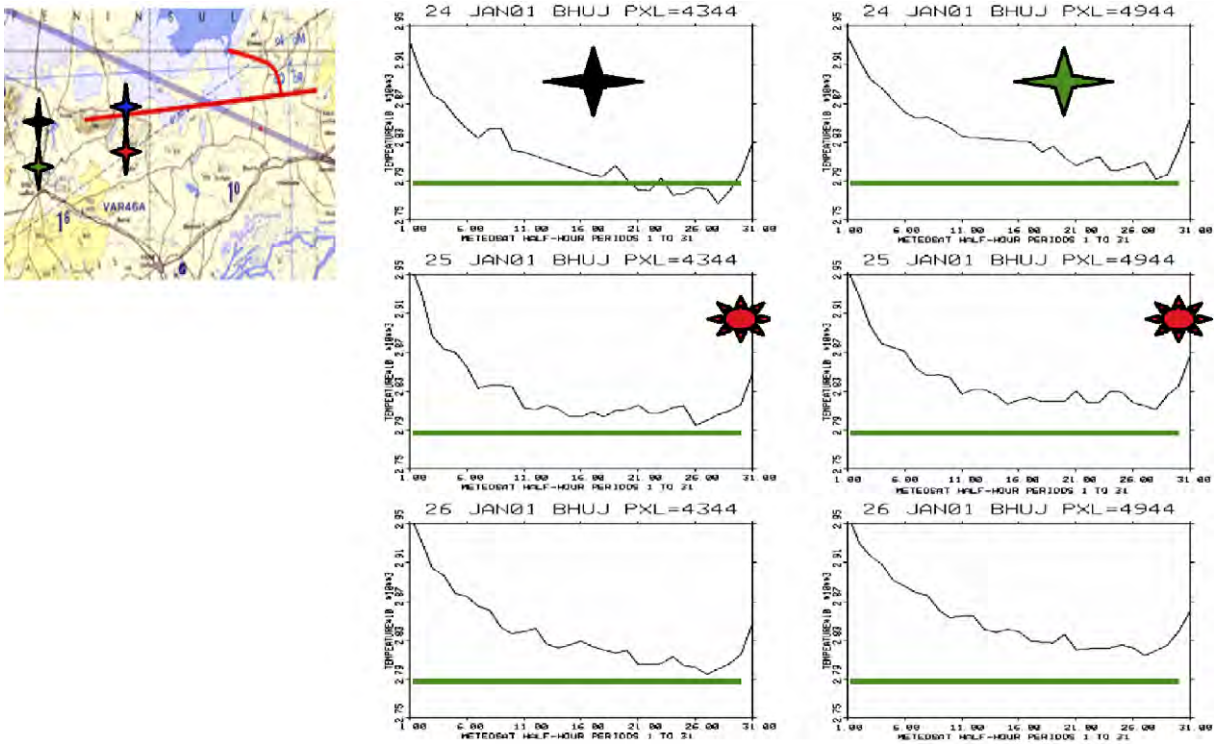

Fig. 3. Time-series temperature plots from Meteosat along the Bhuj, India faults. The plots are for the (in vertical order) evening prior to-, evening of- and evening after- the earthquake events (6 pm to 6 am local time). The green horizontal lines are all at 279 K for Bhuj, providing a relative temperature reference from day to day for each pixel measured. The red stars mark the event time for Bhuj, India. Note the elevated temperatures and the increase in temperature values on the evening of each event relative to the normal temperature declines throughout a night. The mapped areas for India is approximately 150 km × 100 km.

Table 2
Average temperatures and temperature slope regression values observed along and adjacent to Hector Mine M 7.1, Oct 16, 1999, and Bhuj M7.6, Jan 26, 2001 earthquake faults

Fault measurement timeframe	Measures along faul		Measures 8 km away	
	Temp. (K/h)	Reg. slope	Temp. (K/h)	Reg. slope
Hector Mine, CA (Oct 16, 1999 02.47 am local)				
A. 11:00 pm to 02:30 am local time				
Oct 14/5 night before earthquake	288.20	−2.4721	289.21	−2.2771
Oct 15/6 night of earthquake	**287.85**	**−3.1045**	**288.48**	**−3.8872**
Oct 16/7 night after earthquake	280.58	−3.1046	281.43	−3.2991
B. 03:00 am to 06:30am local time				
Oct 14/5 night before earthquake	287.07	−1.9350	288.26	−1.8870
Oct 15/6 night of earthquake	**287.43**	**+0.1090**	**287.86**	**−0.3930**
Oct 16/7 night after earthquake	278.60	−3.1905	279.57	−2.5812
Bhuj, India (Jan 26, 2001 08:46 am local)				
01:30 am to 06:30 am local time				
Jan 24/5 night before earthquake	278.22	−2.2081	279.14	−2.7889
Jan 25/6 night of earthquake	**280.07**	**+0.0094**	**280.52**	**−0.3242**
Jan 26/7 night after earthquake	280.62	−1.9424	280.86	−0.9061

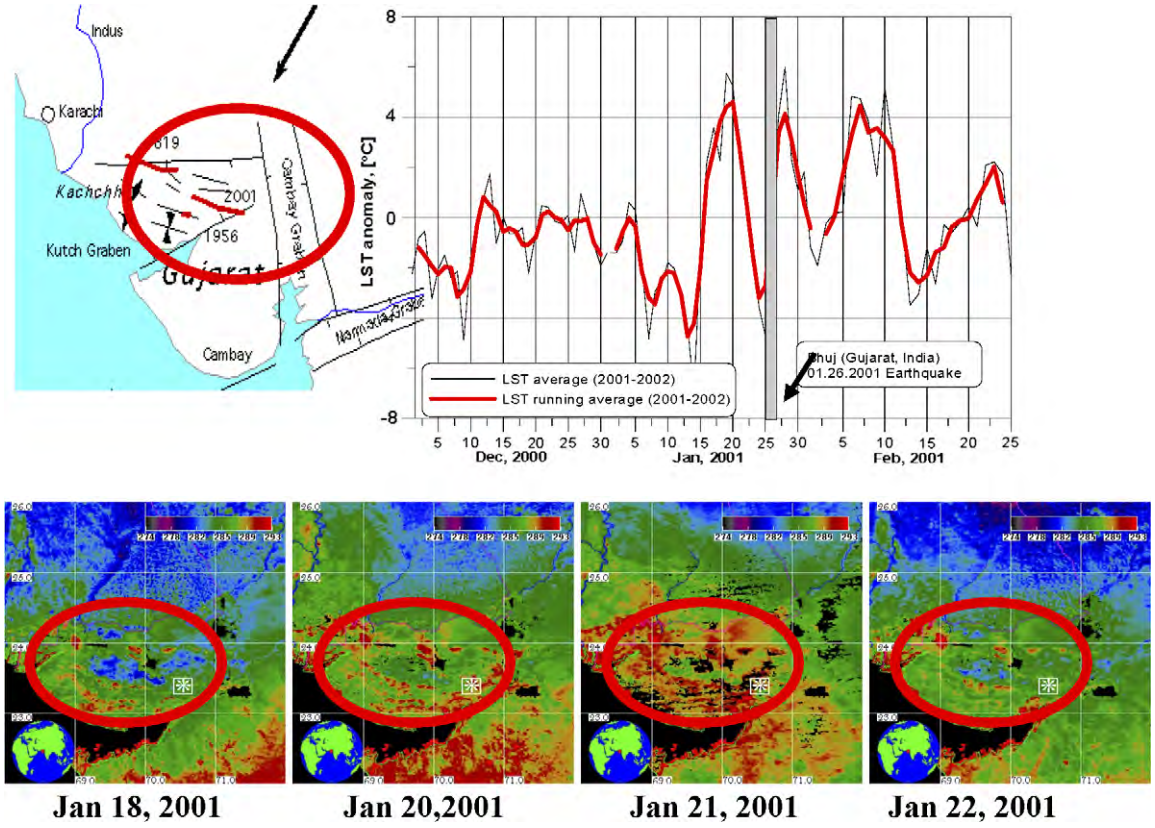

Fig. 4. Time series mean nighttime LST, 100 × 100 km anomaly, comparing 2001 vs 2002 over the Bhuj, Gujarat region, M7.6 January 26, 2001.

high values compared to the background for the three nights of 19–21 January. On the next day emissivity became normal along the faults as can be seen on January 22. This anomaly could be associated with stress related changes of near ground air layer because of the gas release and changing the humidity which also are highly absorbed in the 10–11 μm range.

3.2. Boumerdes, northern Algeria, May 21, 2003, M6.8

The approach used to analyze the Boumerdes strike-slip earthquake using geosynchronous weather data is different from the Bhuj thrust fault event by analyzing the time series measurement of average nightly temperatures and temperature trends at points along the fault line. Temperatures

and temperature trends were also measured away from the fault line to determine the "uniqueness" of the trend in a "thermal anomaly" when compared with the surrounding region. This technique revealed elevated temperatures and regression slope trends on days prior to the event of May 21, 2003, and a "pulse" in apparent heating on May 18, 2003 relative to prior days (see Table 3). Elevated temperatures and a positive trend in temperature regression slopes (Fig. 5) were found along the fault line during the night after the 6:30 pm event.

From the polar orbit satellite data Terra/MODIS crossing Boumerdes at ~10AM, 10PM UTC, and Aqua/MODIS crossing at ~1PM, 1AM UTC have been used for continues time series analysis within 90 days during the main shock. The epicenter was offshore of the coastal city of Boumerdes. We analyzed data include LST and SST during the day and nighttime simultaneously from Terra and Aqua MODIS sensor. Our area of analysis included a radius 50 km around the epicenter and night/days daily scans of LST over the area and computing the LST anomalies using formulas (1) and (2).

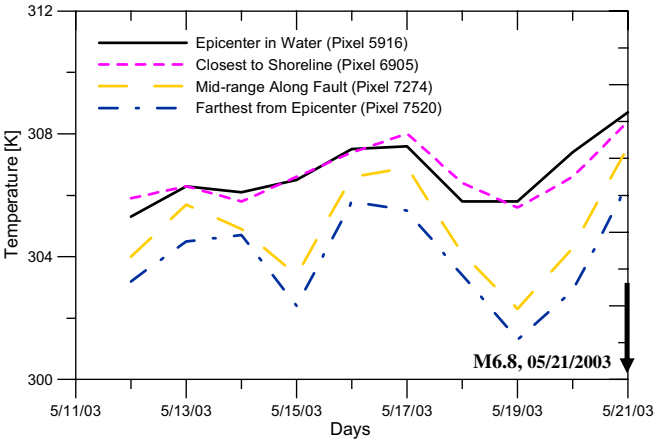

Fig. 5. Average nighttime temperature, of Boumerdes, M6.8, northern Algeria, May 21, 2003.

Table 3
Mean average and average of regression of nightly temperature values, of Boumerdes, northern Algeria, M6.8, May 21, 2003

Date	Along fault	
	Mean average nightly temperature values (K)	Average of regression of nightly temperature values
May 12, 2003	304.78	−1.1216
May17, 2003	304.76	−1.3053
May 18, 2003	**306.83**	**−0.6987**
May 19, 2003	307.05	−2.1555
May 20, 2003	304.71	−1.4549
May 21, 2003	**303.27**	**+0.2388**
May 23, 2003	307.54	−1.6389

We see a thermal infrared (TIR) anomalies pattern (Fig. 6, Terra/MODIS night – red, Aqua/MODIS night – blue), as a maximum of two standard deviation (offset from the average for the region and time) for the entire area, (nighttime) positive temperature excursion compared to the background. The TIR enhancement began on May 16/17, 4–5 days before the event, close to the main tectonic

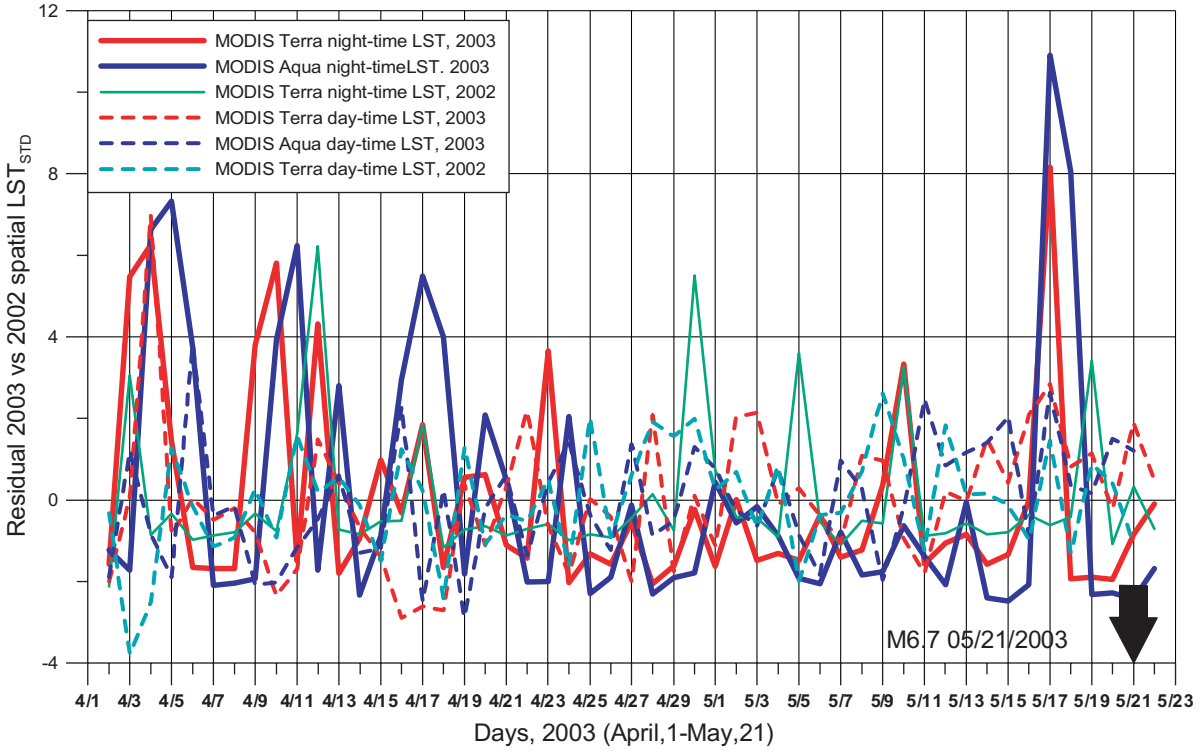

Fig. 6. Time series mean MODIS LST night- and day-time from Terra and Aqua (April–May, 2003/2002) in area of 50 × 50 km around the earthquake of Boumerdes, northern Algeria, M6.8, May 21, 2003.

fault but it did not spread beyond 200 km from the epicenter location. In comparison the level of selected LST anomaly related to year before (2002 Terra/MODIS night – green) and LST during the MODIS/Terra and Aqua day time (dashed lines – red and blue) is 1.5 times bigger in comparison to the biggest LST in the entire time range.

Statistical analysis (see Section 2.2) was preformed to estimate the SST variability during the same period of 90 days around May 21, 2003. In Fig. 7 night images of Terra/MODIS for May 18, 19 and 20 were shown as land was masked with black. Decrease of SST with amplitude −2 °C were observed on location close to the epicenter and this temperature decrease pattern could not be seen before or after the main shock. The statistical analysis confirms that a few days before the main shock there were local up welling of cold water with an average SST −2 °C in comparison with the background mean temperature (Fig. 7).

A possible explanation of SST negative anomalies for shallow sea quakes (water depth <500 m) produced by cold-water upwelling from the sea bottom could be a chaotic turbulence triggered by gas released /heating from the bottom of the ocean and upwelling of cold deep water was proposed as main causes of the observed anomalies (Nosov, 1998; Ouzounov and Freund, 2004).

3.3. Kunlun, Tibet, China, Nov 14, 2001, M7.7

The approach used geosynchronous weather data to analyze the Kunlun, Tibet strike-slip faulting revealed elevated temperatures and regression slope trends on the day prior to the event of November 14, 2001. Temperature trends are probably lower for this event than other event observations, as November is winter in Tibet. Elevated temperatures and a positive trend in temperature regression slopes were found along the fault line during the night after the event (Fig. 8, Table 4).

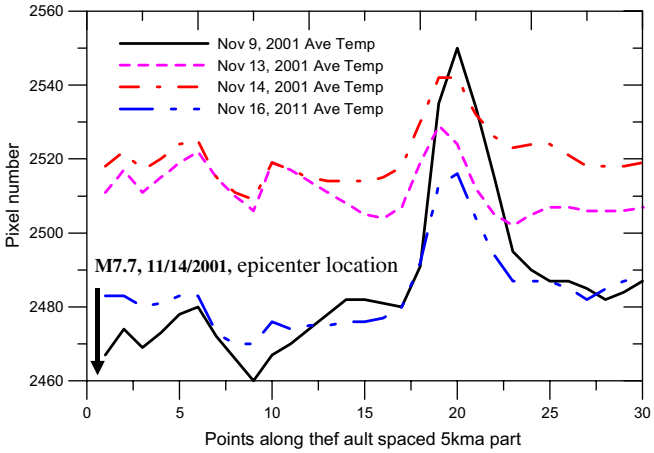

Fig. 8. Average nightly temperatures along the fault, Kunlun, Tibet, China, M7.7, Nov 14, 2001. The horizontal axis shows points along the fault spaced 5 km apart. The first point on the left side of the line (point#1) is at the epicenter of the earthquake. The data points all are located to the East of the epicenter. The large values at points 19–22 overly a large lake that appears along the fault. This data demonstrates how water bodies negate any signal using a time series regression technique due to the high thermal inertia and electromagnetic absorption of water.

3.4. Colima, Mexico, January 21, 2003, M7.8

Using nighttime emissions from the polar orbit satellite data, we have analyzed the LST data over 90 days by

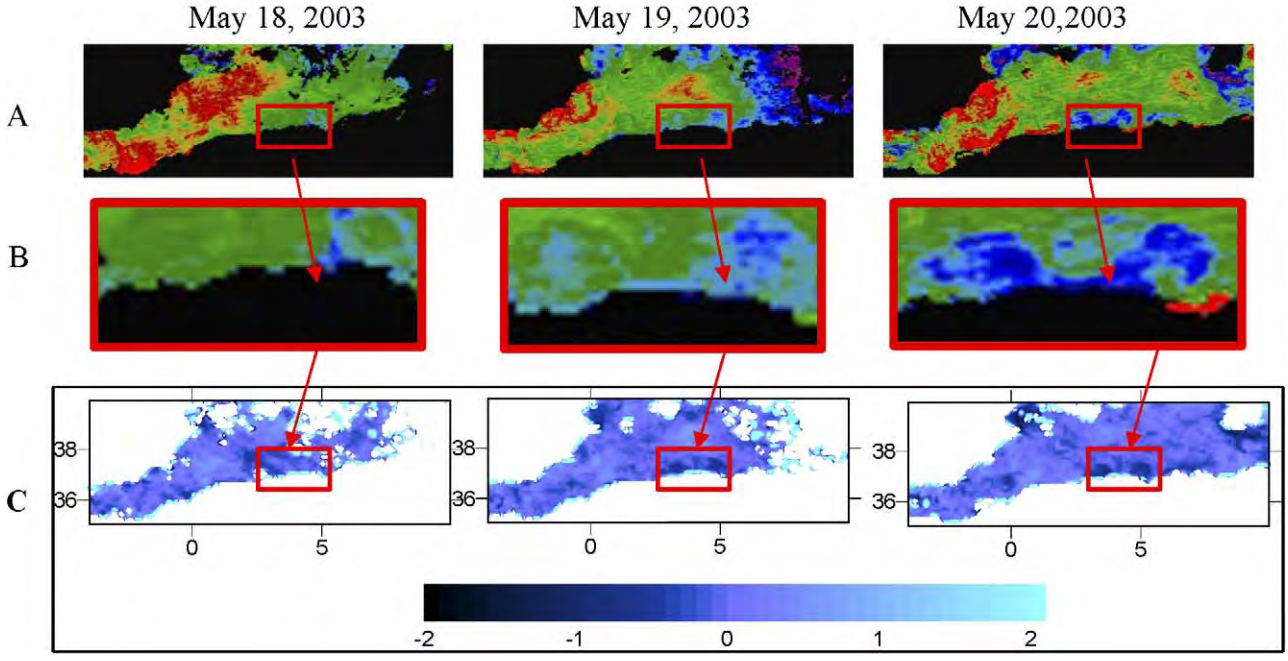

Fig. 7. MODIS Terra LST for May 18, 19 and 20 in near zone to the epicentre. (A) Map of 4.5 km nighttime girded SST data, with red rectangle marking the upwelling area. Land is masked with black color. (B) Zoom in the epicentral area with cooling the surface temperature (blue color). (C) SST residual computed for the same days by the method of median polish for of Boumerdes, North Algeria, M6.8, May 21, 2003.

Table 4
Mean average nightly temperature values, Kunlun, Tibet, China, M7.7, Nov 14, 2001

Date	Along fault				15 km North of fault				15 km South of fault				30 Random points 20–250 km away from fault			
	T^{mean} (K)	σ^T	$Regr^{aver}$	σ^{Ra}	T^{mean} (K)	σ^T	$Regr^{aver}$	σ^{Ra}	T^{mean} (K)	σ^T	$Regr^{aver}$	σ^{Ra}	T^{mean} (K)	σ^T	$Regr^{aver}$	σ^{Ra}
Nov 9, 2001	248.8	21.21	−3.14	0.56	246.6	12.65	−3.58	0.55	248.0	0.91	−3.44	0.47	250.6	23.22	−2.95	0.90
Nov 4, 2001	251.1	6.76	−1.40	0.67	249.4	5.71	−1.89	0.47	251.3	16.52	−1.56	0.43	252.1	18.16	−1.70	0.96
Nov 14, 2001	252.0	7.75	−2.71	0.51	250.9	5.79	−3.65	0.49	252.2	12.13	−2.73	0.33	253.3	17.46	−3.10	0.99
Nov 18, 2001	248.4	11.07	−3.28	0.66	247.3	6.23	−3.40	0.37	248.3	9.41	−3.11	0.33	249.8	21.41	−2.96	0.86

means of the 11–12 μm emissivity ratio covering an area of 100 × 100 km (Pulinets et al., 2006b). For the Colima (Mexico) region the Terra/MODIS day/night crossing time is ~5AM, 5PM UTC, and Aqua/MODIS day/night crossing is close to 8PM, 8AM UTC.

Fig. 9(B) illustrates the variations of the nighttime LST for Terra (black) and nighttime LST for Aqua (red) for the period from December 1, 2002 up to March 1, 2003 for the square 100 × 100 km around the Colima epicenter. On January 15–17, a pronounced LST increase (Fig. 9(B)) is observed for the area close to the epicenter of the January 22 magnitude 7.6 event. To verify the significance of this enhancement we build the yearly LST anomaly between 2002 and 2003 (Fig. 9(B) Terra/MODIS – with light green shaded color, Aqua/MOIDS – dark blue color). In this case the LST anomaly for the area within 100 × 100 km area around the epicenter over a period of 90 days (December 1, 2002–March 1, 2003) is defined as residuals of the two-year data (2002 vs 2003) analysis of time interval of 90 days. One can see the positive increase in the temperature range from January 14, 2002 in comparison to 2003 and the gradual diminishing the day–night temperature difference to the end of January.

Variations of air temperature and Terra/MODIS TIR anomaly for Colima stations are shown in Fig. 9(C) and (B) (black color). The air temperature is derived for 21.25

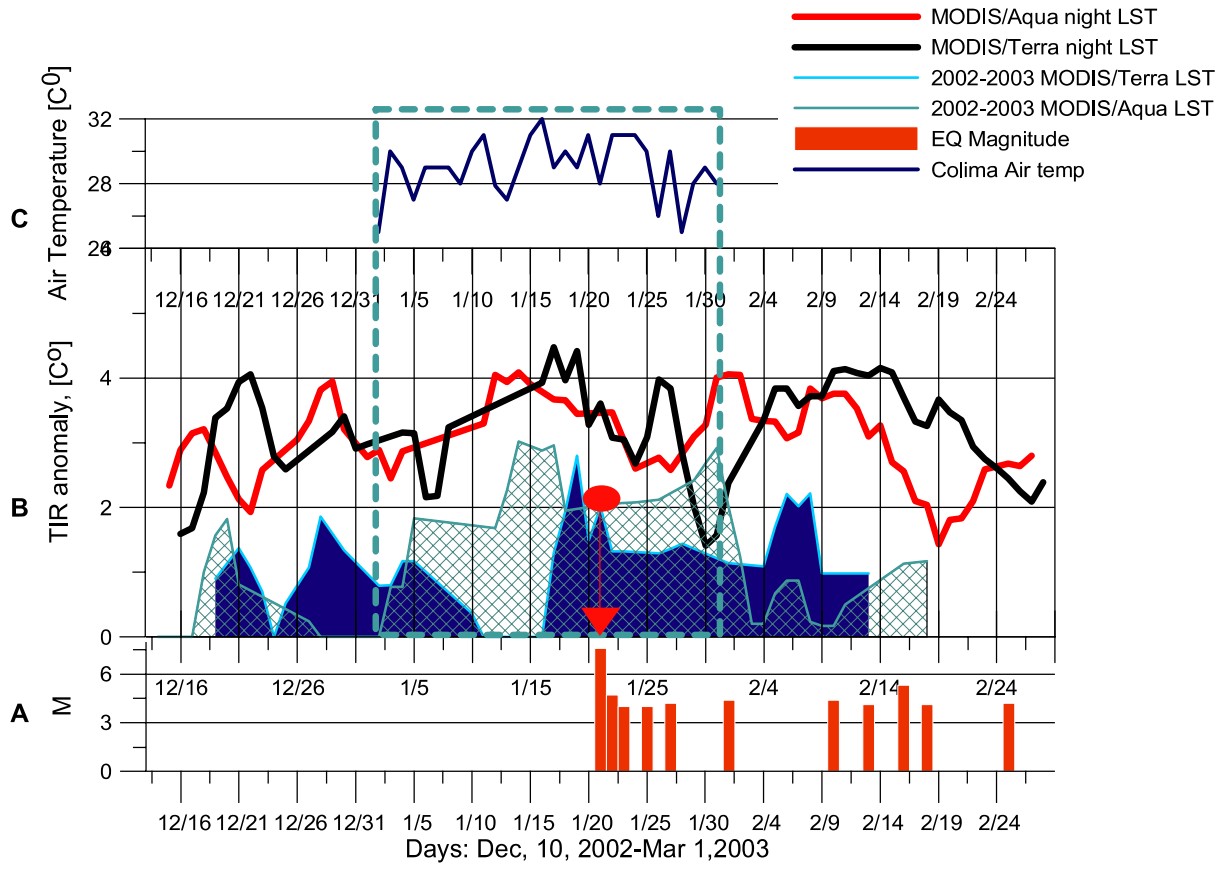

Fig. 9. Colima region for January–February 2003. Variation of seismic activity. (A) MODIS Terra and Aqua (B) and round air temperature (C) analysis around M7.6, Colima, January 22, 2003. (A) Earthquake occurrence for Colima region for Jan–Feb 2003; (B) LST Night time MODIS/Terra (B-black), MODIS/Aqua (B-red) anomaly computed in 100 × 100 km area around the epicenter. 2002–2003 residual of LST anomaly for MODIS/Terra (dark blue) and MODIS/Aqua (light shadow); (C) January 2003 night time air T (°C) into the area of analysis.

LT and synchronized with the passing time for MODIS/Terra satellite for the region. Both air temperature and TIR anomaly curves were fitted with running average windows, (rank 3) show identical time increase (January 15) of air temperature (Colima station) and nighttimes LST for the area (areal estimate for the 100×100 km around the epicentre, which include the Colima station).

4. Conclusions

The complex analysis of TIR satellite data retrieved by polar orbiter and geosynchronous satellite measurement around the time of selected earthquakes demonstrated that the transient TIR anomalies occurred prior to these earthquakes and confirmed the earlier findings. The process starts along the main tectonic fault zone as was shown for Bhuj (India), Kunlun, (China), Boumerdes, (North Algeria) and Colima (Mexico) and variations could be seen in a radius of approximately 100 km around the epicenter over the land and sea. The optimal condition for detecting similar anomalies includes dry weather, clouds free, low vegetation scenes with a long observation baseline. Each of the presented IR techniques has its own advantages – the co-registration approach could mark the elevated temperatures along the fault lines during the nights before and after the events with high temporal resolution, and the areal polar-orbit LST estimate could provide 2-D transient variation of IR emission from surface with 0.5 K accuracy over the global scale. Two independent techniques based on different satellites source confirm the existence of TIR elevations prior to strong earthquakes characterized by different seismo-tectonic settings. This outcome could be used as basis for theoretical studies refining the mechanism of these phenomena and for methodology settings for global monitoring of TIR related to main earthquakes.

Acknowledgements

This work was supported by NASA Grant NNG04GO01G. The authors thank to acknowledge the MODIS science team, LP DAAC and GES DAAC for making their data available to the user community. Thanks are also due to the two anonymous referees for their assistance in evaluating this paper.

References

Bryant, N., Zobrist, A., Logan, T., 2003. Automatic co-registration of space-based sensors for precision change detection and analysis IGARSS 2003 Transactions, Toulouse France, 21–26 July 2003.

Carreno, E., Capote, R., Yague, A., et al., 2001. Observations of thermal anomaly associated to seismic activity from remote sensing. General Assembly of European Seismology Commission, Portugal, 265–269.

Cressie, N., 1993. Statistics for spatial data. Wiley, New York.

Di Bello, G., Filizzola, C., Lacava, T., Marchese, F., Pergola, N., Pietrapertosa, C., Piscitelli, S., Scaffidi, I., Tramutoli, V., 2004. Robust satellite techniques for volcanic and seismic hazards monitoring. Annals Geophys. 47 (1), 49–64.

Fizzola, C., Pergola, N., Pietrapertosa, C., Tramutoli, V., 2004. Robust satellite techniques for seismically active area monitoring: a sensitivity analysis on September 7, 1999 Athens's earthquake. Phys. Chem. Earth 29, 517–527.

Freund, F., 2002. Charge generation and propagation in rocks. J. Geodynamics 33, 545–572.

Gorny, V.I., Salman, A.G., Tronin, A.A., et al., 1988. The Earth's outgoing IR radiation as an indicator of seismic activity. Proc. Acad. Sci. USSR 301, 67–69.

Justice, C., Vermote, E., Townshend, J.R.G., et al., 1998. The moderate resolution imaging spectroradiometer (MODIS): Land remote sensing for global change research. IEEE Trans. Geosci. Remote Sens. 36, 1228–1249.

Liu, Q., Ding, J., Cui, C., 2000. Probable satellite thermal infrared anomaly before the Zhangbei $M = 6.2$ earthquake on January 10, 1998. Acta Seismologica Sinica 13 (2), 203–209.

Nosov, M.A., 1998. Ocean surface temperature anomalies from underwater earthquakes. Volc. Seism. 19, 371–375.

Ouzounov, D., Freund, F., 2004. Mid-infrared emission prior to strong earthquakes analyzed by remote sensing data. Adv. Space Res. 33 (3), 268–273.

Pulinets, S., Ouzounov, D., Karelin, A., Boyarchuk, K., Pokhmelnykh, L., 2006a. The physical nature of thermal anomalies observed before strong earthquakes. Phys. Chem. Earth 31, 143–153.

Pulinets, S., Ouzounov, D., Ciraolo, L., Singh, R., Cervone, G., Leyva, A., Dunajecka, M., Karelin, Boyarchuk, K., 2006b. Thermal, atmospheric and ionospheric anomalies around the time of Colima M7.8 earthquake of January 21, 2003. Annals Geophys. 24, 1–5.

Qiang, Z., Xiu-Deng, X., Chang-Gong, D., 1991. Thermal infrared anomaly – precursor of impending earthquakes. Chinese Sci. Bull. 36 (4), 319–323.

Salman, A., Egan, W.G., Tronin, A.A., 1992. Infrared remote sensing of seismic disturbances. In: Polarization and Remote Sensing. SPIE, San Diego, CA, pp. 208–218.

Singh, R.P., Bhoi, S., Sahoo, A.K., 2002. Changes observed on land and ocean after Gujarat earthquake of January 26, 2001 using IRS data. Int. J. Remote Sens. 23 (16), 3123–3128.

Singh, R., Ouzounov, D., 2003. Earth processes in wake of Gujarat earthquake reviewed from space. EOS 84 (26), 244–246.

Tramutoli, G., Di Bello, N., Pergola, S., 2001. Piscitelli: robust satellite techniques for remote sensing of seismically active areas. Annals Geophys. 44 (2), 295–312.

Tramutoli, V., Cuomo, V., Filizzola, C., Pergola, N., Pietrapertosa, C., 2005. Assessing the potential of thermal infrared satellite surveys for monitoring seismically active areas. The case of Kocaeli (İzmit) earthquake, August 17th, 1999. Remote Sens. Environ. 96 (3–4), 409–426.

Tronin, A., Hayakawa, M., Molchanov, O.A., 2002. Thermal IR satellite data application for earthquake research in Japan and China. J. Geodynamics 33, 519–534.

Tronin, A.A., Biagi, P.F., Molchanov, O.A., Khatkevich, Y.M., Gordeeev, E.I., 2004a. Temperature variations related to earthquakes from simultaneous observation at the ground stations and by satellites in Kamchatka area. Phys. Chem. Earth 29, 501–506.

Tronin, A.A., Molchanov, O.A., Biagi, P.F., 2004b. Thermal anomalies and well observations in Kamchatka. Int. J. Remote Sens. 25 (13), 2649–2655.

Wan, Z., Li, Z.-L., 1997. A physics-based algorithm for retrieving land-surface emissivity and temperature from EOS/MODIS data. IEEE Trans. Geosci. Remote Sens. 35, 980–996.

Yagi, Y., 2001. Western India Earthquake March 9, 2001, University of Tokyo, http://wwweic.eri.u-tokyo.ac.jp/yuji/southindia/.